Viability of an X-Ray Spectrum's Effective Energy for Use in Simulation

Advanced Lab 2023

Seth White, John Meneghini

May 4, 2023

Saint Vincent College
Department of Physics

Abstract

Modern medical imaging using X-rays poses many challenges to doctors concerning the risk of cancer and damage to DNA. By creating a computational model for these x-rays using ray-tracing, the imaging process can be optimized to reduce these health risks. In this study, a monoenergetic effective energy value for X-ray spectra was studied for varying materials, thicknesses, and positions using the NIST attenuation coefficients for future use in a ray-tracing model. When comparing to simulated effective energy curves generated with SpekPy[1], the experimental curves for the monoatomic materials demonstrated a similar, but more rapid, linear relationship, while the compounds demonstrated an anomalous, exponential relationship. Additionally, it was found that varying the thickness and position of materials resulted in unexpected discrepancies in effective energy.

Introduction

X-ray imaging is a critical diagnostic tool used by medical professionals to diagnose and treat various illnesses and injuries. While the use of X-rays is essential to provide immediate, life-saving results, the amount of radiation dosage patients receive can be more than medically necessary. This excessive radiation exposure can increase the risk of cancer, DNA damage, and other potential health risks, making it crucial to minimize the amount of radiation exposure patients receive during X-ray imaging.[2]

While one could minimize radiation dosage by adding shielding and/or changing the position of the target/x-ray source and obtain a reported dosage from the x-ray machine software, this approach has limitations. First, it is time-consuming in often urgent situations, and it still does not guarantee the optimal imaging parameters. Secondly, when it comes to resource-limited settings, the increased cost of imaging procedures due to this optimization procedure may not be financially viable.

To address these challenges, a research project focusing on the development and validation of a computational modeling approach for X-ray attenuation and medical imaging simulation using ray tracing is in progress in Saint Vincent College's Physics Department. This approach will be able to accurately simulate the image one might obtain from an X-ray machine, while also being able to approximate the associated dosage. Accurate computer simulations enable the user to easily add shielding and change the X-ray source orientation, allowing one to optimize the imaging procedure by finding the best quality image that can be obtained with a minimal dosage of ionizing radiation.

In particular, this approach to X-ray simulation uses ray tracing, which is a common graphics technique that simulates particles of light traveling in a 3D environment. It is in this 3D environment that one can place models of objects and trace the path of the light particles through the objects. By using the objects' attenuation coefficient, which is a parameter that describes how strongly a material weakens or reduces the strength of X-rays as they pass through the material, and the distance light travels through the object, one is able to calculate the attenuation of the X-ray and simulate the expected X-ray image.

Currently, this ray-tracing model assumes a single energy x-ray, monoenergetic, is traveling through the objects in the scene; however, with actual X-ray machines, a wide range of energies, polyenergetic, is observed. This observed spectrum has the following explanation: inside an X-ray tube, electrons build up on a filament and are accelerated to an anode as a result of a high voltage being applied across the filament (cathode) and the X-ray target (anode). As the electrons hit the target, often made of tungsten, the electrons have a low probability of being slowed down and deflected by the positive charge of the protons in the target nucleus. The kinetic energy of the electrons lost due to this attraction is converted to an electromagnetic wave of equal energy and increases with proximity to the nucleus. This phenomenon is called *bremsstrahlung radiation* and is the only source of the energy spectrum at a kVp below 69.5 keV. In the extremely rare case that an electron loses all of its kinetic energy due to this nucleus interaction, the maximum energy x-ray is produced and is equal

to the accelerating voltage of the tube, which is referred to as the spectrum's kVp. Once a tube's kVp rises above 69.5 keV, the binding energy of tungsten's K shell, a vacancy will be left in the K shell and electrons from the L shell, which has a binding energy of 11.5 keV, will fill this vacancy, producing an x-ray of energy $69.5 - 11.5 = 57.0$ keV. As a result, as the kVp of the tube increases, intensity spikes as a result of electron transitions will appear in the X-ray energy spectrum.[3]

Therefore, to better model reality, it would be best to redesign the ray-tracing model to produce photons according to an energy distribution; however, this would involve thousands of photons per pixel, which would drastically increase the render time of the simulation. An alternative option would be to find the singular X-ray energy that would result in the same attenuation as a particular energy spectrum produced by a tube, which is called the effective energy.[3] With this energy, one would be able to obtain approximately the same results as the spectrum of energies produced by the x-ray machine, eliminating the need to complicate the model and increase computation time. While this effective energy technique would solve many of the simulation's problems, the factors that affect the effective energy must first be determined.

Methods

In particular, the following factors were tested: an object's composition, geometry (thickness), and position in the X-ray detector. To test any of these factors, one must first determine how to obtain the effective energy, E_{eff}, from an X-ray image. The initial X-ray intensity the moment before encountering the object, I_0, and resulting intensity upon exit, I, are related by the exponential attenuation law:

$$I = I_0 e^{-\mu x}, \tag{1}$$

where μ is the attenuation coefficient of the material and x is the distance the X-ray travels through the material[4].

Solving Equation (1) for μ yields the following relationship:

$$\mu = \frac{\ln\left(I_0/I\right)}{x}. \tag{2}$$

With μ being a function of effective energy, one can refer to experimental data to relate a value of μ to its associated effective energy. Therefore, with NIST's Tables of X-Ray Mass Coeffecients[4] and Equation (2), one can find the I_0, I, and x for a particular x-ray image and determine the effective energy of the spectrum at the set kVp.

To obtain these values, a small surgical X-ray machine called the GE MiniView 6800

Mini C-Arm was used in the anatomy lab at Saint Vincent College, as described in Figure (1). In order to test the composition dependence of the effective energy, images were taken of aluminum (labeled N), iron, magnesium, water, and a plastic scintillator. The thickness and density of each attenuator can be found in Table (1). Several images were taken for each object, with kVps ranging from 40 keV to 60 keV. For each image, the object was placed in the center of the imaging area of the C-Arm, and the kVp was set with the kVp controller located on the machine. Once ready, a remote was used to activate the machine, which then sent X-rays from the tube toward the imaging area.

Attenuator	Thickness (cm)	Density (g/cm^3)
Aluminum (N)	0.23	2.7
Aluminum (I)	0.081	2.7
Iron	0.01	7.87
Magnesium	0.1	1.46
Plastic Scintillator	1.98	1.03
Water	5.80	1.0

Table 1: The thicknesses and denisties of materials used in obtaining effective energy values.

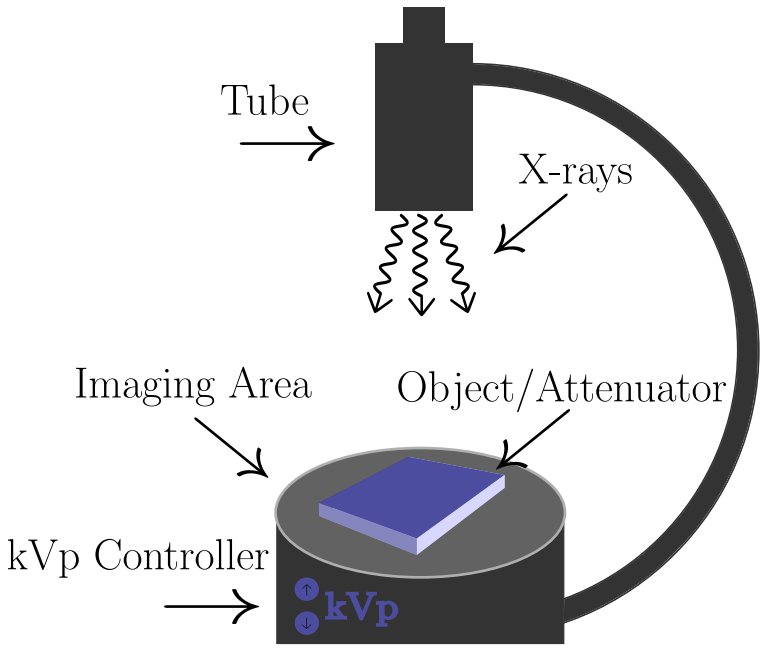

Figure 1: Diagram of GE MiniView 6800 Mini C-Arm used in effective energy measurements.

To test the geometrical dependence of effective energy, an image was taken of a slightly thinner sheet of aluminum (labeled I) and compared to an image of the thicker aluminum

(labeled N) used for the composition experiment. Additionally, for the position dependence, an image was taken of aluminum shifted towards the edge of the imaging area. For both of these experiments, the images taken were compared to images taken at the same kVp to observe only the change in effective energy due to the factors adjusted, rather than a change due to a shift in the spectrum.

With images taken, I/I_0 had to be extracted from each image to determine μ using Equation (2). With I/I_0 acting as the intensity relative to initial intensity, one can think of this ratio as the probability of x-ray transmission. In particular, if we have an arbitrarily large number of photons passing through an object, I/I_0 describes what percentage of particles will pass through (e.g. if equal to 1, all have passed, and if 0, all were attenuated). Similarly, if we imagine a single photon passing through an object, I/I_0 will give the probability of that photon passing through the object. Therefore, if a photon passes through N objects,

$$\frac{I_N}{I_0} = \prod_{j=1}^{N} \frac{I_j}{I_0}, \tag{3}$$

where I_j is the intensity of a ray as it exits the j-th object and I_N is the intensity of a ray as it exits the N-th object.

Consider the X-ray image in Figure (2); along an X-ray's journey from the tube to the detector, it encounters two different attenuators, the air and the object placed in the imaging area (with the machine setting a completely non-attenuated beam equal to 1 in the image, where 1 is white and 0 is black, the only values we can measure from pixel inspection are the relative intensities of the x-ray. Because of this, I will now simply refer to the pixel intensity (0-1) and will replace I/I_0). In the image, I becomes I_{bkg} and I_{ctr} for the pixel intensity in the background and center of the image, respectively. I_{bkg} refers to attenuation caused by the air, while I_{ctr} refers to attenuation caused by both the air and the object. Using Equation (3), one can show that $I_{\text{ctr}} = I_{\text{bkg}} I_{\text{obj}}$, where I_{obj} is the attenuation caused by the object. Therefore, the attenuation caused by the object, and the pixel intensity if there were no attenuation from the air is given by

$$I_{\text{obj}} = \frac{I_{\text{ctr}}}{I_{\text{bkg}}}. \tag{4}$$

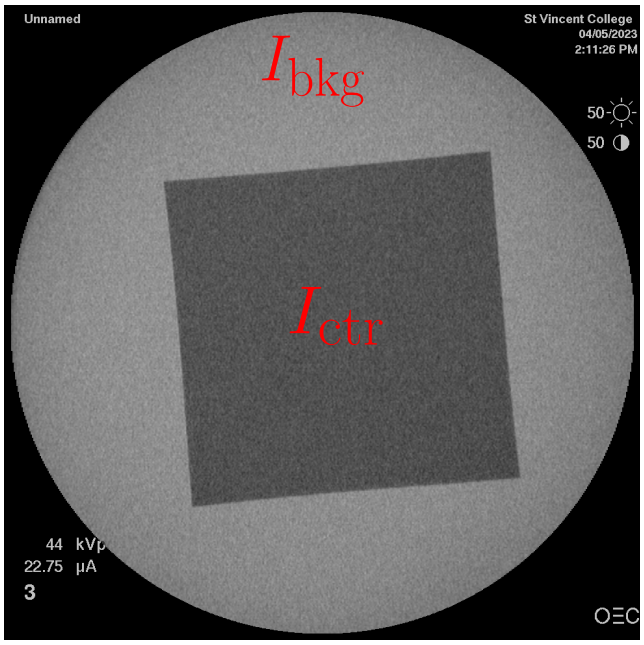

Figure 2: X-ray image of Al at 44 kVp demonstrating the locations of the pixel values used in the calculation of I_{obj}.

To obtain the relative intensity values in the background and center of an image, the average pixel value was taken over a square region in the desired sections of the image. With this relative intensity, extracted with the Python code in Code Listing (1), and the thickness of the object, the attenuation coefficient and effective energy of the interaction were determined using Equation (2) and NIST's database.

Data and Results

To relate the calculated attenuation coefficient of a particular object to the effective energy, a 2nd degree, 4 knot B-spline was used to fit NIST's mass attenuation coefficient data[4], where the mass attenuation coefficient is defined as the attenuation coefficient divided by the object's density, μ/ρ. This fit, implemented with the Python package Scikit-Learn[5], provided $\mu = f(E_{\text{eff}})$; however, $E_{\text{eff}} = f(\mu)$ was needed. The described fits are shown in Figure (3).

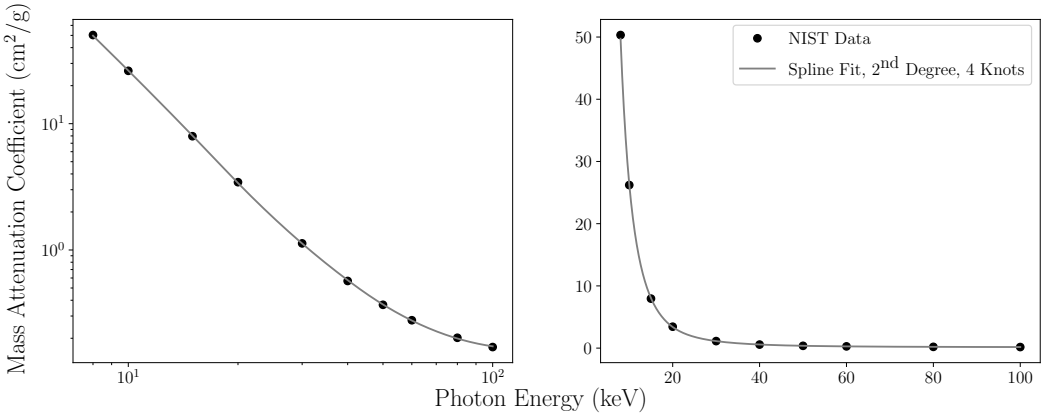

(a) Al

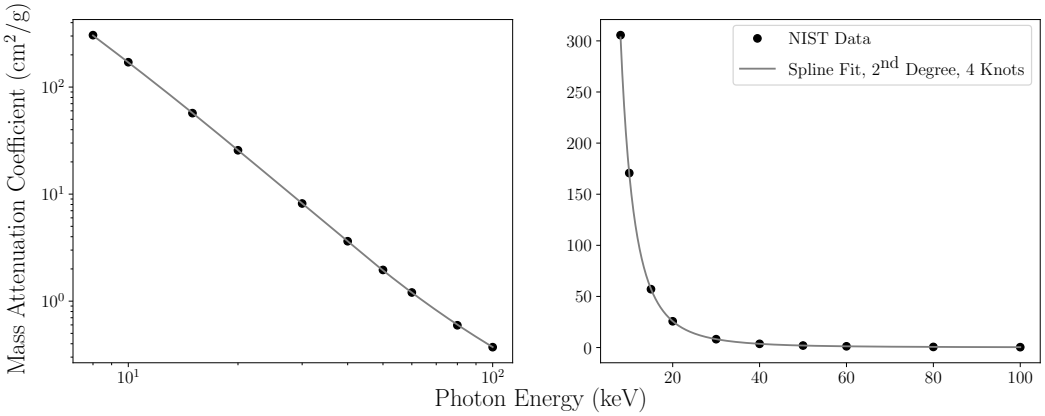

(b) Fe

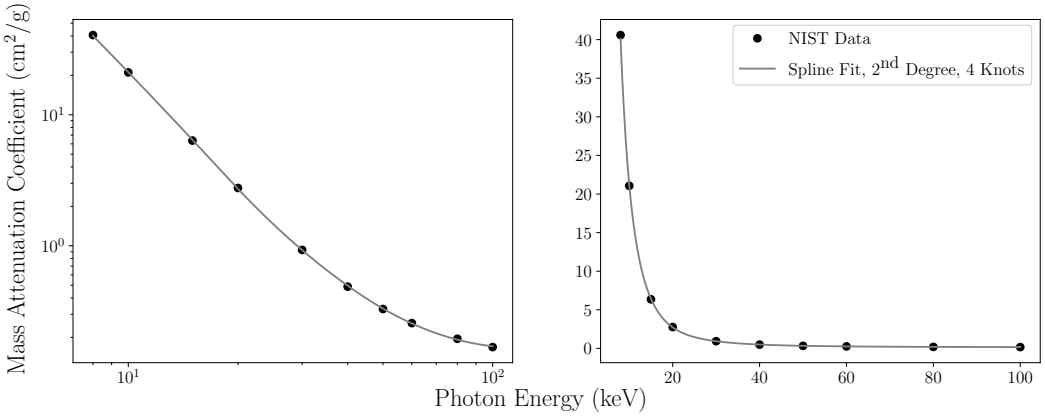

(e) Mg

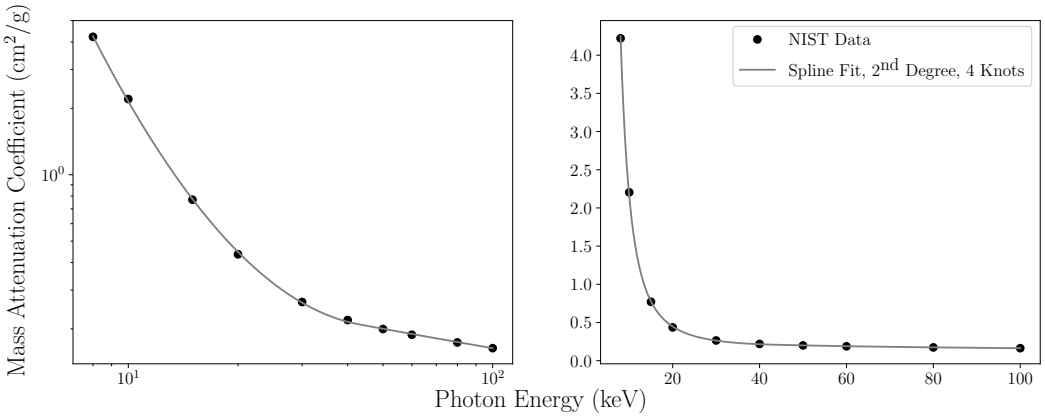

(f) Plastic Scintillator

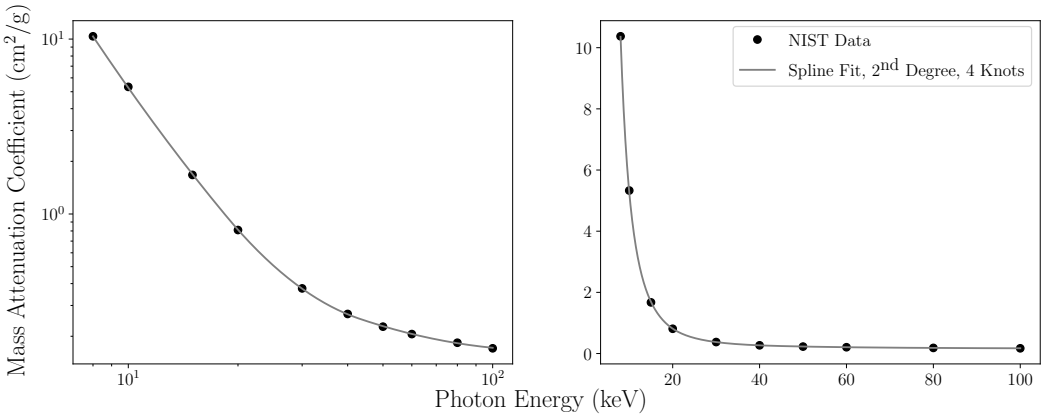

(g) Water

Figure 3: The NIST mass attenuation coefficient data (in cm^2/g) vs. effective energy (in keV) for the Al, Fe, Mg, plastic scintillator, and water fitted using the described B-Spline.

Because f represents an abstract model, an inverse was unable to be taken, so an evenly spaced E_{eff} array of 10,000 values ranging from 0.8 keV to 100 keV was substituted into our model, providing its associated μ/ρ array. Given a particular $\mu/\rho \pm \sigma$, where σ represents the sample standard deviation, Std., of the mass attenuation coefficient, the E_{eff} was found by first determining the index of the element in the μ/ρ array closest to the particular μ/ρ. The associated E_{eff} was then the element in the E_{eff} array located at the determined index. The range of error for a particular E_{eff}, [E_{eff} Min, E_{eff} Max], was calculated by repeating the indexing process for $\mu/\rho + \sigma$ and $\mu/\rho - \sigma$. The results of this indexing technique for each X-ray image can be found in Table (2).

Material	kVp (kV)	I/I_0	I/I_0 Std.	μ/ρ (cm^2/g)	μ/ρ Std. (cm^2/g)	E_{eff} (keV)	E_{eff} Max (keV)	E_{eff} Min (keV)
Aluminum	40.0	0.310	0.025	1.895	0.131	24.552	25.215	23.954
	42.0	0.425	0.026	1.385	0.099	27.635	28.444	26.917
	44.0	0.567	0.025	0.920	0.071	32.576	33.698	31.591
	46.0	0.668	0.023	0.655	0.056	37.747	39.302	36.403
	48.0	0.727	0.023	0.516	0.052	42.145	44.380	40.277
	50.0	0.888	0.020	0.192	0.037	83.926	100.000	69.711
Iron	40.0	0.353	0.030	13.239	1.078	25.316	26.089	24.626
	42.0	0.432	0.031	10.668	0.898	27.331	28.196	26.558
	44.0	0.595	0.030	6.595	0.642	32.392	33.588	31.352
	46.0	0.678	0.027	4.937	0.514	35.870	37.287	34.646
	48.0	0.761	0.028	3.473	0.461	40.599	42.687	38.860
	50.0	0.911	0.024	1.186	0.340	60.335	69.195	54.704
Magnesium	40.0	0.632	0.030	2.638	0.274	20.200	20.982	19.529
	42.0	0.832	0.029	1.054	0.200	28.444	31.058	26.531
	44.0	0.874	0.027	0.776	0.176	32.382	36.412	29.668
	46.0	0.909	0.027	0.551	0.172	37.967	46.193	33.431
	48.0	0.940	0.024	0.353	0.145	48.162	72.627	39.936
Plastic Scintillator	40.0	0.578	0.03	0.268	0.025	29.392	32.861	27.000
	42.0	0.645	0.03	0.215	0.023	40.341	57.906	33.845
Water	44.0	0.059	0.025	0.489	0.075	25.500	28.076	23.669
	46.0	0.220	0.030	0.261	0.024	41.096	46.984	37.369
	48.0	0.325	0.029	0.194	0.015	68.652	86.603	58.403

Table 2: The results for each non-saturated (intensities not equal to 0 or 1) X-ray image for the composition experiment.

The graphs of the E_{eff} for each kVp and material combination can be found in Figure (4). To validate the experimental results, simulated E_{eff} values were obtained with the Python module SpekPy[1], using the X-ray tube assembly specifications as provided by the manufacturer[6].

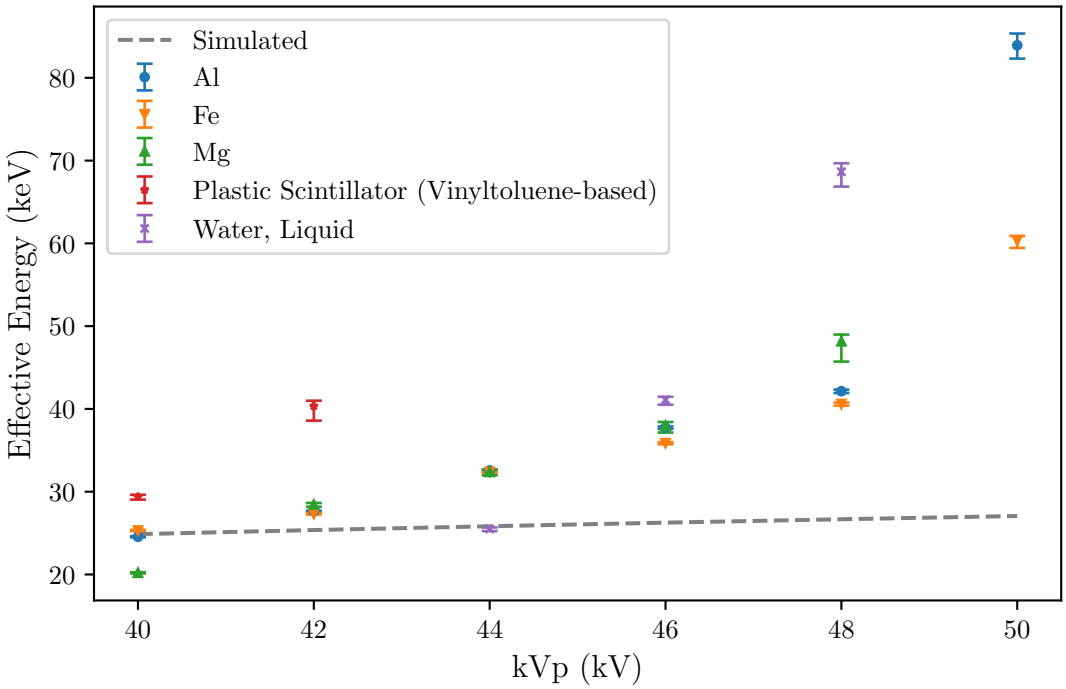

Figure 4: Graph of effective energy (in keV) vs. kVp (in kV) for the X-ray image data contained in Table (2).

Figure (4) shows relative agreement and an approximately linear increase for the Al, Fe, and Mg, up until 50 kVp, where a sudden spike in E_{eff} is observed. For the plastic scintillator and water, vastly different values are observed. Upon further inspection by increasing the range of the fit shown in Figure (3), the two values increase at an exponential rate. Furthermore, the rate of increase of E_{eff} with respect to kVp is greater for the monoatomic attenuators in the experiment compared to their simulated values.

For the offset experiment, the intensity values for the image with the centered Al (labeled N) were obtained with the extraction code in the appendix. On the other hand, the intensity values for the image with the offset Al were obtained manually using the software ImageJ.[7]. The results of this experiment can be found in Table (3)

Position	I/I_0	I/I_0 Std.	μ/ρ (cm^2/g)	μ/ρ Std. (cm^2/g)	E_{eff} (keV)	E_{eff} Max (keV)	E_{eff} Min (keV)
Center	0.310	0.025	1.90	0.13	24.55	25.21	24.00
Offset	0.14	0.05	3.2	0.5	20.5	21.9	19.4

Table 3: The results of X-ray images of a centered and offset Al (labeled N) at 40 kVp for use in the offset experiment.

The results of this experiment show unexpected discrepancies between the centered and offset Al. A slight difference in E_{eff} is expected due to the point-like nature of the x-ray source; however, it can not explain the statistical nonequivalency observed due to the large distance (44.95 cm)[6] between the x-ray source and detector; therefore, demonstrating a dependence on the object's position in the imaging area for the E_{eff}.

For the thickness-varying experiment, x-ray images of Al were taken at 40 kVp. The thickness of the Al was varied by using two different attenuators, one of thickness 2.286 mm (labeled N) and the other of thickness 0.813 mm (labeled I), as found in Table (1). The intensity values for each image were obtained with the code in Code Listing (1). The results of this experiment can be found in Table (4).

Thickness (mm)	I/I_0	I/I_0 Std.	μ/ρ (cm^2/g)	μ/ρ Std. (cm^2/g)	E_{eff} (keV)	E_{eff} Max (keV)	E_{eff} Min (keV)
2.286	0.310	0.025	1.90	0.13	24.55	25.21	24.00
0.813	0.575	0.029	2.52	0.23	22.15	22.92	21.39

Table 4: The results of X-ray images of Al (labeled N) and Al (labeled I) at 40 kVp for use in the thickness-varying experiment.

The results of this experiment, once again, show unexpected discrepancies in E_{eff} between the two thicknesses. While the E_{eff}'s are closer than what was measured for the offset experiment, the two values are statistically nonequivalent; therefore, demonstrating a thickness dependence of the E_{eff}.

Discussion

The discrepancies between E_{eff} for the monoatomic materials and the compounds have been explored extensively with little resolution. Several different theories have been explored, including the thickness of the sample, possible code errors, and the normalization of the image.

Upon looking for differences between the compounds and monoatomic materials, it was observed that both the compounds had a significantly larger thickness than the monoatomics, as seen in Table (1). It was then considered whether or not the increased height of the sample could lead to an increased probability of X-rays scattering off the object and onto the detector. This effect would result in a seemingly larger background and could lead to unexpected E_{eff} values. Upon manual examination of the images, the background was affected; however, the difference in intensity was minor and could not reasonably result in the exponential increase that was measured, especially since the discrepancies are still present in images where the background is non-existent.

Furthermore, since weighted averages of monoatomic attenuation coefficients were

taken in the data processing code to obtain the attenuation coefficients for the compounds, it was considered whether or not a possible error was present in the code that could lead to this exponential behavior. Upon careful examination of the code, no errors were found, and for extra reassurance, a few images of the compounds were manually inspected, and verified the processing code's results.

Additionally, it was found that *Heine & Thomas* (2008)[8] performed a similar E_{eff} calibration using a mammography system. While their overall technique was similar to the methodology of this experiment, one key difference was the normalization factor used in the processing of the intensity data. In particular, they normalized the pixel value by mAs, which is the tube current multiplied by the exposure time. This effectively would be the incident intensity of the x-rays and is equivalent to I_0. However, this normalization was not able to be done for this experiment, since the C-arm does not provide any data on the exposure time for images. Still, this normalization would be the same for each kVp; therefore, this cannot explain the drastic differences between the E_{eff}'s of the monoatomic and compound materials that were measured at higher kVps. On the other hand, since the current of the tube was provided for each image and increased at a rate proportional to the kVp, this could explain why the E_{eff}'s of the monoatomic materials increased at a rate greater than what was predicted by the simulation.

Finally, combining these results with the unexpected differences in E_{eff} that were measured in the offset and varied thickness experiments, it is possible the x-ray machine may be doing some sort of post-processing of the images that are not described in the manual[6]. Without knowing the specifics of this processing, the original, unfiltered images can not be calculated. Overall, the measurements obtained from this experiment reveal that the E_{eff} approach for ray-tracing cannot be used for the GE MiniView 6800 Mini C-Arm. As an alternative, research collaborator Dr. Gregory Bisignani has offered us his clinical X-ray machine for use in further experimentation. Likely, this offer will be accepted and the experiment described in this report will be repeated with his machine.

References

[1] Gavin Poludniowski, Artur Omar, Robert Bujila, and Pedro Andreo. Technical Note: SpekPy v2.0—a software toolkit for modeling x-ray tube spectra. *Medical Physics*, 48 (7):3630–3637, July 2021. ISSN 0094-2405, 2473-4209. doi: 10.1002/mp.14945. URL `https://onlinelibrary.wiley.com/doi/10.1002/mp.14945`.

[2] Kenji Kamiya, Kotaro Ozasa, Suminori Akiba, Ohstura Niwa, Kazunori Kodama, Noboru Takamura, Elena K Zaharieva, Yuko Kimura, and Richard Wakeford. Long-term effects of radiation exposure on health. *The Lancet*, 386(9992):469–478, August 2015. ISSN 01406736. doi: 10.1016/S0140-6736(15)61167-9. URL `https://linkinghub.elsevier.com/retrieve/pii/S0140673615611679`.

[3] J Anthony Seibert. X-Ray Imaging Physics for Nuclear Medicine Technologists. Part 1: Basic Principles of X-Ray Production. *JOURNAL OF NUCLEAR MEDICINE TECHNOLOGY*, 32(3), 2004.

[4] J. H. Hubbell and S. M. Seltzer. X-Ray Mass Attenuation Coefficients, 2004.

[5] F. Pedregosa, G. Varoquaux, A. Gramfort, V. Michel, B. Thirion, O. Grisel, M. Blondel, P. Prettenhofer, R. Weiss, V. Dubourg, J. Vanderplas, A. Passos, D. Cournapeau, M. Brucher, M. Perrot, and E. Duchesnay. Scikit-learn: Machine learning in Python. *Journal of Machine Learning Research*, 12:2825–2830, 2011.

[6] Ge Mini View 6800 Mini C-Arm. *Soma Technology Inc.*

[7] Caroline A Schneider, Wayne S Rasband, and Kevin W Eliceiri. NIH Image to ImageJ: 25 years of image analysis. *Nature Methods*, 9(7):671–675, July 2012. ISSN 1548-7091, 1548-7105. doi: 10.1038/nmeth.2089. URL `http://www.nature.com/articles/nmeth.2089`.

[8] John J. Heine and Jerry A. Thomas. Effective x-ray attenuation coefficient measurements from two full field digital mammography systems for data calibration applications. *BioMedical Engineering OnLine*, 7(1):13, March 2008. ISSN 1475-925X. doi: 10.1186/1475-925X-7-13.

Appendix

```python
def get_relative_intensity(path, background_intensity=0):
    """
    Calculates the relative intensity of a square in the center of an image.
    :param path: Path to image
    :param background_intensity: Intensity of background
    :return: Relative intensity
    """
    # load image
    img = cv2.imread(path, 0)

    # convert to float and normalize
    img = img.astype(np.float32)/255

    # get mean pixel value and std dev of square in center of image
    center = (int(img.shape[0]/2), int(img.shape[1]/2))
    length = 100
    square = img[int(center[0]-length/2):int(center[0]+length/2),
    int(center[1]-length/2):int(center[1]+length/2)]

    mean, std = cv2.meanStdDev(square)

    # if intensity is 1 or 0, return False, so they are not used as data points
    if mean[0][0] >= 0.999 or mean[0][0] <= 0.001:
        return False

    # obtain relative intensity by normalizing by background intensity
    # (I_square = I_background * I_object -> I_object = I_square / I_background)
    mean[0][0] = mean[0][0] / background_intensity


    # convert image to rgb
    img = cv2.cvtColor(img, cv2.COLOR_GRAY2RGB)

    # draw red square on image and relative intensity and std on image
    cv2.rectangle(img, (int(center[0]-length/2), int(center[1]-length/2)),
     (int(center[0]+length/2), int(center[1]+length/2)), (0, 0, 255), 3)

    cv2.putText(img, f"Intensity: {mean[0][0]:.3f} +- {std[0][0]:.3f}",
    ↪  (int(center[0]-length/2),
                int(center[1]-length/2)-10), cv2.FONT_HERSHEY_SIMPLEX, 1, (0, 0,
                ↪  255), 2)

    return ufloat(mean[0][0], std[0][0])
```

Code Listing 1: X-ray image relative intensity extraction code implemented in Python3.